Saltwater as the energy source for low-cost, safe rechargeable batteries

Article *in* Journal of Materials Chemistry A · March 2016

DOI: 10.1039/C6TA01274D

CITATIONS
20

READS
26,075

5 authors, including:

Senthilkumar Baskar
Amrita Vishwa Vidyapeetham
75 PUBLICATIONS **1,854** CITATIONS
SEE PROFILE

Kyoungho Kim
Ulsan National Institute of Science and Technology
12 PUBLICATIONS **323** CITATIONS
SEE PROFILE

Soo Min Hwang
Ulsan National Institute of Science and Technology
81 PUBLICATIONS **2,611** CITATIONS
SEE PROFILE

Youngsik Kim
Seowon University
173 PUBLICATIONS **15,194** CITATIONS
SEE PROFILE

Journal of Materials Chemistry A

PAPER

Cite this: J. Mater. Chem. A, 2016, 4, 7207

Saltwater as the energy source for low-cost, safe rechargeable batteries†

Sangmin Park,‡ Baskar SenthilKumar,‡ Kyoungho Kim, Soo Min Hwang* and Youngsik Kim*

Received 11th February 2016
Accepted 29th March 2016

DOI: 10.1039/c6ta01274d

www.rsc.org/MaterialsA

The effective use of electricity from renewable sources requires large-scale stationary electrical energy storage (EES) systems with rechargeable high-energy-density, low-cost batteries. We report a rechargeable saltwater battery using NaCl (aq.) as the energy source (catholyte). The battery is operated by evolution/reduction reactions of gases (mostly O_2, with possible Cl_2) in saltwater at the cathode, along with reduction/oxidation reactions of Na/Na^+ at the anode. The use of saltwater and the Na-metal-free anode enables high safety and low cost, as well as control of cell voltage and energy density by changing the salt concentration. The battery with a hard carbon anode and 5 M saltwater demonstrated excellent cycling stability with a high discharge capacity of 296 mA h $g_{hard\ carbon}^{-1}$ and a coulombic efficiency of 98% over 50 cycles. Compared with other battery types, it offers greatly reduced energy cost and relatively low power cost when used in EES systems.

Introduction

The harvest and storage of electrical energy from renewable sources have become increasingly important due to many reasons: the growing demand for electricity, a steady increase in oil price, fossil fuel depletion, and environmental considerations such as global warming from CO_2 emission.[1] Most green energy is harvested from natural sources such as wind, thermal, and solar power. Supplying electrical energy directly from these sources is difficult as the energy is still costly and not always available where and when it is needed.[2] The development of large-scale, efficient electrical energy storage (EES) systems is highly desirable as it can help mitigate fossil-fuel related environmental issues and provide a solution to peak load in power supply by saving the energy during off-peak times and releasing it during on-peak times.[3–5]

Lithium-ion batteries (LIBs) combine high energy density (250–300 W h kg^{-1}), reasonable cost (250–400 \$ kW h^{-1}), and long service lifetimes (2–10 years).[4,6] However their wide application in portable electronic devices and electric vehicles may strain lithium production capability and increase their market price in the long term.

Na-based batteries have gained much interest as candidates for post-LIBs. Not only is sodium abundant and low-cost, it also has a suitable electrochemical potential ($E^\circ = -2.71$ V *vs.* the standard hydrogen electrode, SHE).[7–9] Na–air batteries have been studied intensively because their theoretical energy density (1100–2080 W h kg^{-1}) is high compared with that of existing LIBs.[10–13] Aqueous Na–air batteries possess especially good reversibility owing to their soluble discharge product NaOH, compared to aprotic Na–air batteries whose discharge products are insoluble Na_2O_2 and/or NaO_2.[10,14–16] Nevertheless, the repeated plating and stripping of the Na metal anode during cycling would reduce this reversibility, impeding further development of aqueous Na–air batteries. It can also cause safety issues, due to its high reactivity with the electrolyte and resultant dendritic growth.[9,17,18]

Our group has recently developed a new 'seawater battery'[19–21] as a hybrid between a battery and a fuel cell. The seawater battery uses natural seawater containing Na^+ as the catholyte, making its application in large-scale, stationary EES systems environmentally friendly and price-competitive. Anode materials such as hard carbon or other Na-insertion materials are also safer as they are free of Na metal.[19] However, the use of seawater limits the EES plants to coastal locations. The amount of Na^+ in seawater (approximately 0.46 M) also limits the battery energy density.[22]

In this work, we demonstrate an alternative 'saltwater battery', using the more available NaCl aqueous solution as the catholyte. This is distinct from existing saltwater batteries, where the saltwater only serves as an electrolyte between two galvanically coupled electrodes. Our saltwater battery could offer significantly reduced production cost, which is one prerequisite for large-scale EES systems, together with the removal of the geographical limitation. The battery consisting of a hard carbon anode and 5 M saltwater catholyte showed

School of Energy and Chemical Engineering, Ulsan National Institute of Science and Technology (UNIST), 50 UNIST-gil, Ulsan 689-798, Republic of Korea. E-mail: ykim@unist.ac.kr; smhwang@unist.ac.kr

† Electronic supplementary information (ESI) available. See DOI: 10.1039/c6ta01274d

‡ These authors contributed equally to this work.

a high discharge capacity of 296 mA h g^{-1} and good cycling performance, with a coulombic efficiency of 98% over 50 cycles. Our results suggest that this saltwater battery should be a promising candidate for low-cost, grid-scale stationary EES systems.

Results and discussion

Design and key components of the saltwater battery

The saltwater battery stores electrical energy based on the electrochemical reactions of the NaCl aqueous solution, which is easily available at low cost. The battery structure and its charge/discharge processes are illustrated in Fig. 1a and b. The anode and cathode compartments are separated by a ceramic solid electrolyte. The cathode part contains only a current collector and saltwater, which is used as the Na^+ source as well as the catholyte. For the positive current collector, a hydrophilic network-structured carbon paper consisting of numerous microfibers is employed (Fig. 1d). It provides a large surface area with many reaction sites, together with good wettability (Fig. 1d, inset). The hydrophilic carbon paper significantly reduced the overpotentials arising from the charge/discharge processes, compared to a hydrophobic one (Fig. S1, ESI†). The anode part consists of Na metal or sodium-insertion materials (*e.g.* hard carbon) as the negative electrode[23,24] and 1 M $NaCF_3SO_3$ in tetra ethylene glycol dimethyl ether (TEGDME) as the liquid organic electrolyte.

For the solid electrolyte, a Na super ionic conductor, $Na_3Zr_2Si_2PO_{12}$ (NASICON) ceramic, is used to separate the cathode and anode parts and allows the selective transport of Na^+. The crystal structure of the synthesised NASICON pellet was identified by X-ray diffraction (XRD) (Fig. S2, ESI†), which showed a typical NASICON phase of the monoclinic structure with the *C*2/*c* space group (JCPDS #35-0412).[25] Fig. 1e exhibits the plan-view scanning electron microscopy (SEM) image, in which the grain boundaries are clearly visible.[26] The appearance and size of the pellet can be seen in the inset digital image. The density of the NASICON pellet was measured to be 3.14 g cm^{-3}, which is 96% of its theoretical density of 3.27 g cm^{-3}.[27] The Nyquist plot of the NASICON pellet at 25 °C (Fig. 1f) showed a depressed semicircle in the high frequency region and a linear spike in the low frequency region, which indicates a typical ionic conductor characteristic. From the measured impedance data, the ionic conductivity was evaluated to be approximately 1.0 mS cm^{-1} (the bulk and grain boundary terms were 2.9 and 1.0 mS cm^{-1}, respectively), which is similar to ionic conductivities reported in the literature.[15,27,28] The prototype saltwater battery cell was assembled with the aforementioned components and then immersed in saltwater before electrochemical testing (Fig. 1c).

Reaction mechanism and the effect of salt concentration

Using saltwater (containing Na^+ and Cl^- ions and H_2O) as the catholyte, the saltwater battery experiences evolution/reduction reactions of gaseous phases, specifically the oxygen evolution reaction (OER)/oxygen reduction reaction (ORR) and chlorine evolution reaction (CER)/chlorine reduction reaction (CRR) at the cathode during charge/discharge processes (Fig. 1a).[19–21] On

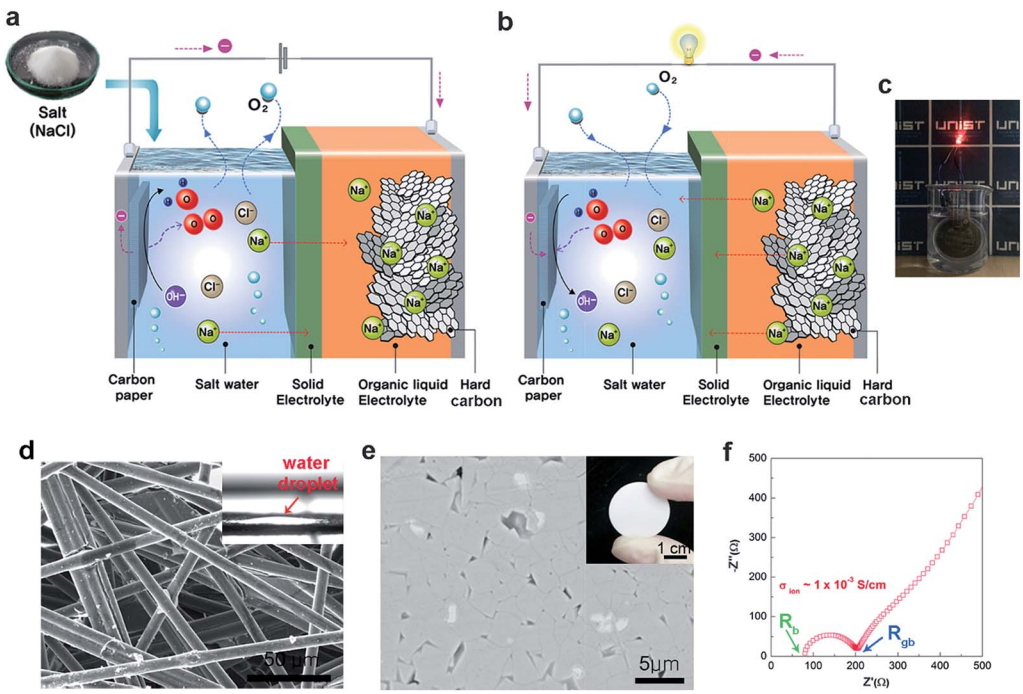

Fig. 1 Cell structure and key components of the rechargeable saltwater battery. Schematics showing the (a) charge and (b) discharge processes of the saltwater battery. (c) Photograph of the saltwater battery lighting an LED bulb. (d) SEM image of the hydrophilic carbon paper (HCP) used as the current collector, showing its wettability (inset). (e) Plan-view SEM image of the NASICON pellet, and a photograph showing its actual size (inset). (f) Nyquist plot of the NASICON pellet.

the anode side, sodium ions are transported from the catholyte through NASICON and reduced to Na metal during charging, whereas discharging oxidises Na metal and returns Na^+ to the catholyte. Since saltwater (1 M) has a neutral pH (~7), the following two types of overall reactions can be expected, during charging

$$4NaCl\ (aq) + 2H_2O\ (l) \rightarrow 4Na\ (s) + O_2\ (g) + 4HCl\ (aq);\ E^\circ = 3.53\ V\ (pH = 7) \quad (1)$$

$$2NaCl\ (aq) \rightarrow Cl_2\ (g) + 2Na\ (s);\ E^\circ = 4.07\ V \quad (2)$$

and during discharging

$$4Na\ (s) + 2H_2O\ (l) + O_2\ (g) \rightarrow 4NaOH\ (aq);\ E^\circ = 3.53\ V\ (pH = 7) \quad (3)$$

According to the reaction potentials, the OER route (reaction (1), 3.53 V) is thermodynamically favourable than the CER route (reaction (2), 4.07 V) during charging. However, the CER has been reported to occur together with the OER in NaCl (aq) due to the latter's high overpotential.[29,30] This implies the possibility of the CER during the charging process in our saltwater batteries.

First, we investigated the first galvanostatic charge and discharge curves of the battery with 1 M saltwater at a current rate of 0.025 mA cm^{-2} (Fig. 2a, purple curve). The charge and discharge voltage plateaus were found to be 3.84 and 2.72 V, from which the overpotentials were estimated to be 0.31 and 0.81 V, respectively. The discharge overpotential was relatively large compared to the charge overpotential. The pH of saltwater was maintained ~7 throughout the charge/discharge processes. Since the measured charge voltage was lower than the theoretical potential of the CER (4.07 V), the main electrochemical reaction during charging would be the OER rather than the CER. Our previous studies on seawater batteries showed the evidence of the CER during charging, as the concentration of Cl^- decreased with the charging time.[20] In this study we also observed that the concentration of Cl^- decreased monotonically with increasing charging time for the battery with 0.4 M saltwater, which is comparable to the NaCl concentration in seawater (Fig. S3, ESI†).

To further investigate the occurrence of the CER and OER in saltwater during charging, we measured the cyclic voltammogram (CV) of 1 M NaCl (aq) using a three-electrode half-cell at a scan rate of 10 mV s^{-1} and compared it to that obtained using 1 M Na_2SO_4 (aq). The latter has no Cl^- ions, therefore no CER would occur.[31] As shown in Fig. 2b, within a potential window of 0–1.1 V *vs.* SHE (2.7–3.8 V *vs.* Na^+/Na), 1 M NaCl displayed a couple of redox current signals with a voltage difference, which could be assigned to the OER and ORR in the anodic and

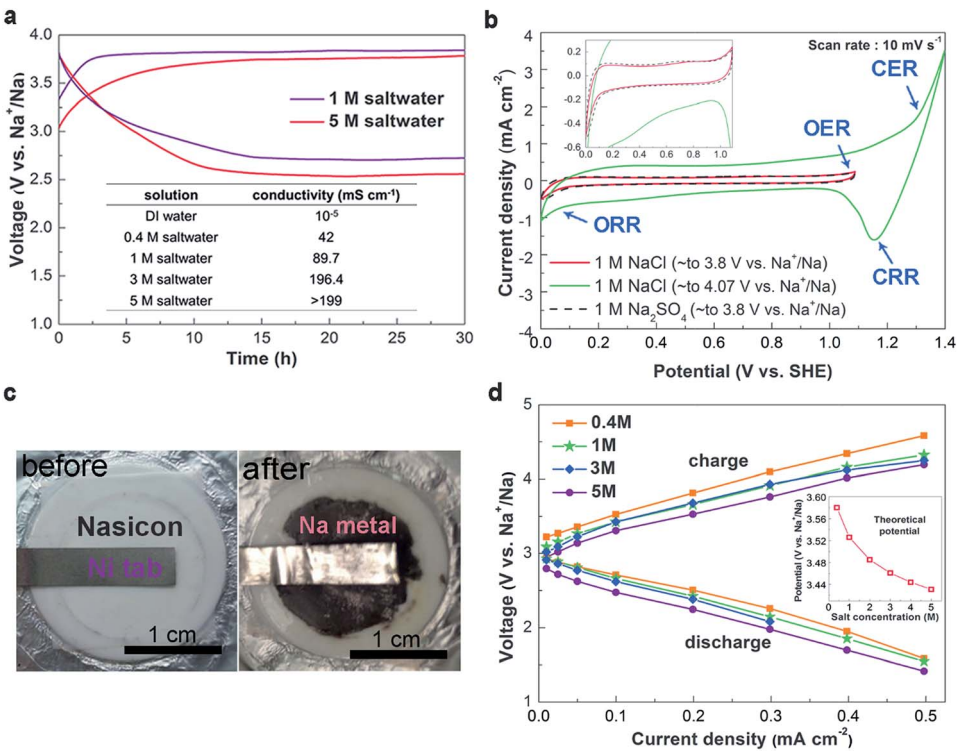

Fig. 2 Reaction mechanism and salt concentration effect. (a) Galvanostatic charge and discharge voltage profiles of (Na|saltwater) half-cells with 1 M and 5 M saltwater at a current rate of 0.025 mA cm^{-2}. Inset: the ion conductivities of saltwater at various concentrations. (b) Cyclic voltammograms of 1 M saltwater and 1 M Na_2SO_4 aqueous solution at a scan rate of 10 mV s^{-1}. An enlarged portion (inset) shows no notable difference between two sets of CV curves. (c) Photographs of the anode side before and after charging over 200 h at a current rate of 0.1 mA cm^{-2}, showing dark areas of Na metal deposition. (d) Polarisation plots of the half-cells with different salt concentrations as a function of the current rate (0.01–0.5 mA cm^{-2}). The inset indicates the theoretical redox potentials with respect to the salt concentration.

cathodic directions, respectively. On the other hand, the CV curve within a potential window of 0–1.4 V *vs.* SHE (2.7–4.1 V *vs.* Na^+/Na, green curve in Fig. 2b) reveals significantly larger anodic currents and an additional reduction peak (at approximately 1.15 V *vs.* SHE) in the cathodic scan. The increased current appears to be a result of the CER[32] in addition to the OER, and the reduction peak corresponds to the CRR.[31,33] Based on the CV results and the galvanostatic charge–discharge voltage profile, we consider the saltwater battery charges mainly by the OER due to the electrolysis of the saltwater at the cathode side, although the CER cannot be completely ruled out. The dominance of the OER is also corroborated by the CV result of 1 M Na_2SO_4 (Fig. 2b, dashed line), which is very close to that of 1 M NaCl. Parallel to the oxidation of saltwater by the OER, Na^+ ions dissolved in the catholyte are transferred to the anode side through NASICON and then reduced to Na metal. After charging for 200 h at a current rate of 0.1 mA cm^{-2}, the anode showed pure Na metal extracted from saltwater (dark areas in Fig. 2c, for EDS results see Fig. S4, ESI†), demonstrating the usability of saltwater as a Na^+ containing active material.

Next, we examined the effect of salt concentration on the electrochemical properties of saltwater batteries. Fig. 2d displays the polarisation graphs of saltwater batteries with 0.4, 1, 3, and 5 M NaCl. The voltage points were obtained by averaging the voltage profile measured at various current densities for 1 h. At all concentrations, the charge voltage increased while the discharge voltage decreased with increasing current density, thus widening the charge–discharge voltage gap. Increasing the concentration of NaCl caused a larger decrease in the charge voltage, whereas the discharge voltage was rather decreased (refer to comparison between the 1 M and 5 M results in Fig. 2a). We measured the ionic conductivity of the saltwater at the corresponding concentrations (Fig. 2a, inset). Generally, the high ionic conductivity of the electrolyte in batteries enhances kinetics of the redox reaction and thereby enables a decrease in the charge voltage, while an increase in the discharge voltage, as a result of reduced ohmic resistance. The increase of ionic conductivity by increasing the salt concentration (within the range of 0.4–5 M), however, had a negligible effect on the charge and discharge voltages. Instead, the theoretical redox potential (Fig. 2d, inset) is the main factor in determining the charge/discharge voltages of saltwater batteries.

Electrochemical performances of the saltwater battery

The electrochemical performance of the Na-metal-free saltwater battery is first examined through half-cells: an anode half-cell with a hard carbon electrode and a cathode half-cell with saltwater. As a representative sodium-intercalation material, hard carbon exhibits a high reversible capacity (250–300 mA h g^{-1}) and a low sodium-ion-insertion potential (<1.0 V *vs.* Na^+/Na).[34,35] Hard carbon as the negative electrode can thus avoid poor reversibility (cyclability) stemming from the dendritic growth of Na metal during cell operation. Theoretically, the energy density of saltwater batteries is dependent on the concentration of NaCl (catholyte) and the capacity of the anode. Considering the maximum solubility of NaCl in water (6 M at 25 °C) and the stability of the NaCl solution at room temperature, we assembled a half-cell saltwater battery with a 5 M saltwater catholyte (Na|5 M saltwater), whose theoretical energy density was calculated to be 368 W h kg^{-1} (for details see the ESI†). For the anode, we evaluated the electrochemical properties of a hard carbon electrode using a 2032 coin-type half-cell (Na|hard carbon). The galvanostatic charge–discharge profiles at a current rate of 0.025 mA cm^{-2} (approximately 26 mA $g_{hard\ carbon}^{-1}$) are shown in Fig. S5 (ESI†). The hard carbon electrode delivered initial discharge (sodiation) and charge (desodiation) capacities of 557 and 370 mA h g^{-1}, respectively, with an irreversible capacity decay of 187 mA h g^{-1} during the first cycle. The low initial coulombic efficiency (66%) could be ascribed to the formation of the solid-electrolyte interphase (SEI) on the hard carbon surface and the trapping of a small amount of Na^+ in the hard carbon.[36] After five cycles, the hard carbon electrode displayed a reversible capacity of 350 mA h g^{-1}.

Fig. 3a exhibits the galvanostatic charge and discharge curves of the cathode and anode half-cells. The cathode half-cell (Na|5 M saltwater) showed charge and discharge voltage plateaus at 3.76 V and 2.56 V, respectively. In the case of the anode half-cell, the charge–discharge profiles were based on the 5th charge–discharge profiles of the coin-type half-cell (Na|hard carbon). Next, we constructed the full-cell saltwater battery (hard carbon|5 M saltwater) and investigated its performance. The full-cell saltwater battery was tested at a current rate of 0.025 mA cm^{-2} with a capacity cut-off condition of 300 mA h $g_{hard\ carbon}^{-1}$ upon charging, and a voltage cut-off condition of 0.5 V upon discharging (Fig. S6, ESI†). At the first cycle, the saltwater battery displayed a considerably low discharge capacity of 46 mA h g^{-1} (initial coulombic efficiency 15%), which was attributed mainly to the formation of the SEI layer during charging (sodiation). It was assumed that during the first charging, most of the input charge (300 mA h $g_{hard\ carbon}^{-1}$) was consumed to form the SEI on the surface of the hard carbon anode. Indeed, the first charge voltage profile of the full-cell corresponded to the sloping region (1.2–0.1 V) of the initial discharge voltage profile of the anode half-cell (Na|hard carbon) (Fig. S5, ESI†). Such a sloping region has been recognised as caused by SEI formation, as well as Na^+-insertion within the graphene layers of hard carbon.[36] As the cycling continued, the discharge capacity steadily increased and the charge–discharge voltage profiles became saturated at the 7th cycle. Fig. 3b exhibits the 7th charge–discharge voltage profile, which was close to the voltage profiles predicted from the two half-cell voltage profiles in Fig. 3a (orange curves). The average charge and discharge voltages of the full-cell were 2.78 V and 2.45 V, respectively.

To examine the Na^+ insertion from the saltwater catholyte into the hard carbon anode, the anode surface of the full-cell disassembled after the 8th charge process was examined by SEM with energy-dispersive X-ray spectroscopy (EDS). The EDS mapping data (Fig. 3c) revealed an increased amount of Na element with uniform distribution after cycling compared to the pristine electrode, which only showed a weak Na signal from the remnant $NaCF_3SO_3$ salt. Fig. 3d shows the cycling performance of the full-cell saltwater battery at a current density of

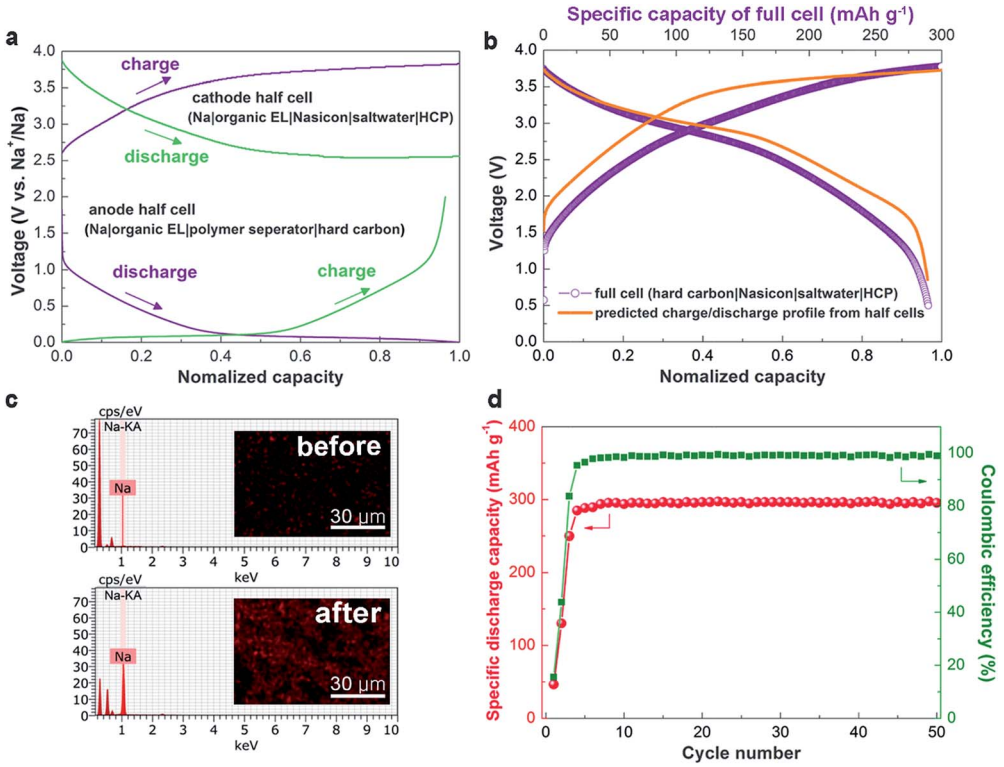

Fig. 3 Electrochemical performance of the rechargeable saltwater battery. (a) Galvanostatic charge and discharge voltage profiles of the cathode and anode half-cells at a current rate of 0.025 mA cm^{-2}; the cathode half-cell employs 5 M saltwater, while the anode is a hard carbon electrode. (b) Purple: the 7th charge and discharge curves of the full-cell (hard carbon|5 M saltwater) at a current rate of 0.025 mA cm^{-2}. The orange curves depict the prediction from the two half-cell results in panel (a). (c) EDS mapping results of the hard carbon anode before cycling, and after the 8th charge process. (d) Cycling performance of the full-cell over 50 cycles.

0.025 mA cm^{-2} over 50 cycles. Although the discharge capacity was initially quite low, it increased with the cycling number and reached a saturation level of 294 mA h g^{-1} by the 7th cycle, reaching a high coulombic efficiency of 98.2%. This behaviour is different from that observed in conventional rechargeable batteries, where initially, the discharge capacity decreases with increasing cycle number by testing with voltage cut-off conditions at constant currents upon both charging and discharging. In contrast, our full-cell saltwater batteries were examined with a capacity cut-off condition of 300 mA h $g_{\text{hard carbon}}^{-1}$, which is lower than the estimated reversible capacity of the hard carbon electrode upon charging. This controlled testing could avoid unwanted Na plating (dendrite formation) on the anode surface during the charging of the full-cell, and consequently allow more stable cycling performance. The full-cell displayed excellent cycling stability without significant capacity fading during 50 cycles. The discharge capacity after the 7th cycle was between 294 and 296 mA h g^{-1} and the coulombic efficiency was maintained at 98% over 50 cycles. Even after 50 cycles, no noticeable XRD peak shift was observed for the NASICON pellet (Fig. S7, ESI†), indicating its stability.

We checked the power density of a saltwater battery with 5 M saltwater (Na|5 M saltwater) by varying the current rate from 0.01 to 0.75 mA cm^{-2} (Fig. S8, ESI†). At 0.5 mA cm^{-2}, a maximum power density of 0.77 mW cm^{-2} was reached, which was significantly low for practical applications. The poor power output could be limited by the ionic conductivity of the solid electrolyte (NASICON), which may benefit from further development of solid electrolytes of high ionic conductivity.

Cost evaluation of the saltwater battery

Fig. 4 illustrates the energy cost *versus* power cost of various types of batteries for EES systems (for details see Table S1, ESI†). Sodium–sulphur batteries (NaS) and vanadium redox flow

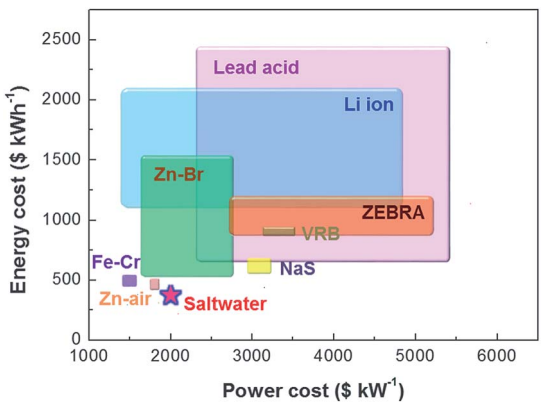

Fig. 4 Comparison of cost for various battery systems. Energy cost ($ kW h^{-1}) *versus* power cost ($ kW^{-1}) using data from DOE/EPRI 2013 Electricity Storage Handbook.[3] The cost of saltwater battery (red star) was evaluated using 5 M saltwater as the catholyte. For details see the ESI.†

batteries (VRB) have been considered as promising candidates for EES systems in addition to LIBs.[2,3] NaS has an energy cost of 438–477 \$ kW h^{-1} and the energy cost of VRB is higher. The energy cost of the saltwater battery with 5 M NaCl is estimated to be only 189 \$ kW h^{-1}; while zinc–air batteries, the next cheapest candidate, is priced at 310 \$ kW h^{-1}. The saltwater batteries are remarkably low-cost in terms of both energy and power production. In addition, the working potential and energy density (up to 423 W h kg^{-1} with 6 M saltwater) of the saltwater battery can be tuned by the salt concentration for different applications.

Conclusions

We have developed a new type of rechargeable saltwater battery, which is distinct in that saltwater acts as the energy source, not just the electrolyte. It is operated by evolution/reduction reactions of gaseous phases in saltwater at the cathode, along with reduction/oxidation reactions of the dissolved Na^+ ions at the anode. Galvanostatic charge–discharge and CV measurements indicated that the OER mainly occurs during the charge process; however, given the monotonic decrease of the Cl^- concentration in saltwater with charging time, the possibility of the CER cannot be excluded. We are currently investigating the evolved O_2 and Cl_2 gases and their ratio during charging, using advanced analytical tools such as customised cells equipped with a differential electrochemical mass spectrometer. The full-cell saltwater battery (hard carbon|5 M saltwater) exhibited a high discharge capacity with a stable capacity retention and a high coulombic efficiency of 98% over 50 cycles. As a conceptually simple energy storage device, this battery using the eco-friendly, low-cost saltwater as the active material will be an optimal building block for large-scale stationary EES applications.

Experimental

Preparation of the saltwater battery

For the catholyte, 60 mL saltwater was prepared by dissolving NaCl (Sigma Aldrich) in deionised water at various concentrations of 0.4–5 M. For the cathode current collector, a Ti mesh (Wooilmetal Corporation) and a sheet of hydrophilic carbon paper (Fuel Cell store) were used. A 0.8 mm-thick NASICON-type solid electrolyte ($Na_3Zr_2Si_2PO_{12}$) with a diameter of 16 mm was prepared according to previous studies.[16,19–21] For the anode compartment, the solid electrolyte was mounted on the open-structured anode top holder and then sealed with the anode bottom holder, which contained an organic electrolyte of 1 M $NaCF_3SO_3$ (Sigma Aldrich) in TEGDME (Sigma Aldrich) and a Ni tap (anodic current collector, Solbrain LTK) attached to the Na metal or hard carbon electrode. The assembly process was carried out in a glovebox under a high-purity Ar atmosphere (O_2 and H_2O less than 1 ppm). The hard carbon electrode was prepared from a slurry of hard carbon (MeadWestvaco Corporation), carbon black Super-P (TIMCAL), and polyvinylidene fluoride (PVdF, Sigma Aldrich) at a weight ratio of 80 : 10 : 10. The slurry was coated on Cu foil (14 μm thick) with a doctor-blade, and dried in a convection oven. Finally, the electrode was roll-pressed and dried in a vacuum oven. The loading level of hard carbon was approximately 2.44 mg cm^{-2}. The assembled cells which consisted of the Ni tap|anode|organic electrolyte|NASICON|saltwater|carbon paper|Ti mesh were immersed in saltwater for electrochemical tests.

Characterisation and electrochemical measurements

The phase identification was carried out by using an XRD (D/Max, Rigaku apparatus) equipped with a Cu Kα X-ray source ($\lambda = 1.5406$ Å). X-ray photoelectron spectroscopy (XPS, Mg Kα, Thermo Fisher) and contact angle measurements (Phoenix 300, SEO) were performed to examine the surface chemistry and wettability of carbon paper, respectively. The surface morphology and microstructure were observed by using a SEM (verios 460, FEI company) equipped with an EDS (Bruker). In order to check Na^+ insertion in the anode side after charging, the cells were carefully disassembled and the electrode was rinsed with a TEGDME solvent and then dried in a vacuum chamber. The Cl^- concentration in saltwater was determined by using an ion chromatography system (Dionex ICS 3000). The density of the solid electrolyte was measured by using a gas displacement pycnometry system (AccuPyc 1340, Micromeritics Instrument Corp.). The ionic conductivities of the solid electrolyte and saltwater were evaluated by electrochemical impedance spectroscopy (EIS, BioLogic) in the frequency range of 100 mHz to 7 MHz and a voltage amplitude of 14.2 mV.

Cyclic voltammetry (CV, BioLogic) was performed using a three-electrode cell and the CV curves were recorded at a scan rate of 10 mV s^{-1}. A carbon paper electrode was used as the working electrode, and an Ag/AgCl electrode (3 M NaCl, 0.197 V *vs.* SHE) and a Pt wire were used as the reference and counter electrodes, respectively. The electrochemical properties of saltwater batteries were measured by using a battery cycler (WBCS 3000, Wonatech) at room temperature. The batteries were galvanostatically charged and discharged at current rates of 0.01–0.5 mA cm^{-2}. The hard carbon anode was examined at a current rate of 0.025 mA cm^{-2} in the voltage window of 0–2 V *vs.* Na^+/Na over 5 cycles. The full-cell saltwater batteries were tested at a current rate of 0.025 mA cm^{-2} with a capacity cut-off of 300 mA h $g_{\text{hard carbon}}{}^{-1}$ upon charging, and a voltage cut-off of 0.5 V upon discharging.

Acknowledgements

This work was supported by the 2015 Research Fund (1.150034.01) of the UNIST (Ulsan National Institute of Science and Technology) and the Energy Efficiency & Resources Core Technology Program of the Korea Institute of Energy Technology Evaluation and Planning (KETEP) granted financial resource from the Ministry of Trade, Industry & Energy, Republic of Korea (No. 20142020104190).

Notes and references

1 M. Z. Jacobson, *Energy Environ. Sci.*, 2009, **2**, 148–173.

2 Z. Yang, J. Zhang, M. C. Kintner-Meyer, X. Lu, D. Choi, J. P. Lemmon and J. Liu, *Chem. Rev.*, 2011, **111**, 3577–3613.
3 A. A. Akhil, G. Huff, A. B. Currier, B. C. Kaun, D. M. Rastler, S. B. Chen, A. L. Cotter, D. T. Bradshaw and W. D. Gauntlett, *DOE/EPRI 2013 Electricity Storage Handbook in Collaboration with NRECA*, Sandia National Laboratories Albuquerque, NM, USA, 2013.
4 B. Dunn, H. Kamath and J.-M. Tarascon, *Science*, 2011, **334**, 928–935.
5 P. J. Hall and E. J. Bain, *Energy Policy*, 2008, **36**, 4352–4355.
6 B. D. McCloskey, *J. Phys. Chem. Lett.*, 2015, **6**, 3592–3593.
7 B. L. Ellis and L. F. Nazar, *Curr. Opin. Solid State Mater. Sci.*, 2012, **16**, 168–177.
8 H. Pan, Y.-S. Hu and L. Chen, *Energy Environ. Sci.*, 2013, **6**, 2338–2360.
9 M. D. Slater, D. Kim, E. Lee and C. S. Johnson, *Adv. Funct. Mater.*, 2013, **23**, 947–958.
10 T. Hashimoto and K. Hayashi, *Electrochim. Acta*, 2015, **182**, 809–814.
11 P. Hartmann, C. L. Bender, M. Vračar, A. K. Dürr, A. Garsuch, J. Janek and P. Adelhelm, *Nat. Mater.*, 2013, **12**, 228–232.
12 S. Ha, J. K. Kim, A. Choi, Y. Kim and K. T. Lee, *ChemPhysChem*, 2014, **15**, 1971–1982.
13 N. Ortiz-Vitoriano, T. P. Batcho, D. G. Kwabi, B. Han, N. Pour, K. P. C. Yao, C. V. Thompson and Y. Shao-Horn, *J. Phys. Chem. Lett.*, 2015, **6**, 2636–2643.
14 K. Hayashi, K. Shima and F. Sugiyama, *J. Electrochem. Soc.*, 2013, **160**, A1467–A1472.
15 F. Liang and K. Hayashi, *J. Electrochem. Soc.*, 2015, **162**, A1215–A1219.
16 S. H. Sahgong, S. Senthilkumar, K. Kim, S. M. Hwang and Y. Kim, *Electrochem. Commun.*, 2015, **61**, 53–56.
17 V. Chevrier and G. Ceder, *J. Electrochem. Soc.*, 2011, **158**, A1011–A1014.
18 B. Senthilkumar, Z. Khan, S. Park, I. Seo, H. Ko and Y. Kim, *J. Power Sources*, 2016, **311**, 29–34.
19 H. Kim, J.-S. Park, S. H. Sahgong, S. Park, J.-K. Kim and Y. Kim, *J. Mater. Chem. A*, 2014, **2**, 19584–19588.
20 J.-K. Kim, F. Mueller, H. Kim, D. Bresser, J.-S. Park, D.-H. Lim, G.-T. Kim, S. Passerini and Y. Kim, *NPG Asia Mater.*, 2014, **6**, e144.
21 J. K. Kim, E. Lee, H. Kim, C. Johnson, J. Cho and Y. Kim, *ChemElectroChem*, 2015, **2**, 328–332.
22 E. Brown, A. Colling, D. Park, J. Phillips, D. Rothery and J. Wright, *Seawater: its Composition, Properties and Behaviour*, Butterworth-Heinemann, 1995.
23 S. Komaba, W. Murata, T. Ishikawa, N. Yabuuchi, T. Ozeki, T. Nakayama, A. Ogata, K. Gotoh and K. Fujiwara, *Adv. Funct. Mater.*, 2011, **21**, 3859–3867.
24 V. Palomares, M. Casas-Cabanas, E. Castillo-Martínez, M. H. Han and T. Rojo, *Energy Environ. Sci.*, 2013, **6**, 2312–2337.
25 J. Boilot, G. Collin and P. Colomban, *Mater. Res. Bull.*, 1987, **22**, 669–676.
26 A. Kuriakose, T. Wheat, A. Ahmad and J. Dirocco, *J. Am. Ceram. Soc.*, 1984, **67**, 179–183.
27 S.-M. Lee, S.-T. Lee, D.-H. Lee, S.-H. Lee, S.-S. Han and S.-K. Lim, *J. Ceram. Process. Res.*, 2015, **16**, 49–53.
28 O. Bohnke, S. Ronchetti and D. Mazza, *Solid State Ionics*, 1999, **122**, 127–136.
29 H. Abdel-Aal, S. Sultan and I. Hussein, *Int. J. Hydrogen Energy*, 1993, **18**, 545–551.
30 H. Abdel-Aal, K. Zohdy and M. A. Kareem, *Open Fuel Cells J.*, 2010, **3**, 1–7.
31 S. Chen, Y. Zheng, S. Wang and X. Chen, *Chem. Eng. J.*, 2011, **172**, 47–51.
32 A. R. Zeradjanin, N. Menzel, W. Schuhmann and P. Strasser, *Phys. Chem. Chem. Phys.*, 2014, **16**, 13741–13747.
33 M. V. Makarova, J. Jirkovský, M. Klementová, I. Jirka, K. Macounová and P. Krtil, *Electrochim. Acta*, 2008, **53**, 2656–2664.
34 D. Stevens and J. Dahn, *J. Electrochem. Soc.*, 2000, **147**, 1271–1273.
35 D. Stevens and J. Dahn, *J. Electrochem. Soc.*, 2001, **148**, A803–A811.
36 E. Irisarri, A. Ponrouch and M. Palacin, *J. Electrochem. Soc.*, 2015, **162**, A2476–A2482.